Check for updates

Isoelectronic Pt(ɪɪ) complexes of cyclometalating C^N^N ligands with phenyl/(benzo)thiophenyl and pyridyl/(benzo)thiazolyl moieties†

Maren Krause, [ID] [a] Joshua Friedel, [ID] [a] Stefan Buss, [ID] [b] Dana Brünink, [c] Annemarie Berger, [ID] [a] Cristian A. Strassert, [ID] *[b] Nikos L. Doltsinis [ID] *[c] and Axel Klein [ID] *[a]

A series of cyclometalated Pt(ɪɪ) complexes [Pt(C^N^N)X] (X = Cl, C≡CPh, C≡CC₆F₅) was synthesised from the protoligands HC^N^N containing either phenyl (ph), naphthyl (na) or (benzo)thiophenyl (b(th)) **C aryl** functions and either pyridyl (py) or (benzo)thiazolyl ((b)tz) **peripheral N** units, alongside the central 4-phenyl-pyridyl (ppy) or *t*Bu₂-phenyl-pyridyl (tbppy) **N** group. Depending on the combination of the **peripheral N** or **C aryl** building blocks, these square planar complexes reveal very different electrochemical, UV-vis absorption and emission behaviour. The reversible reductions shift anodically along the series th/py < ph/tz ≈ th/tz < ph/btz while the irreversible oxidations shift cathodically along the series Cl ≈ C≡CC₆F₅ < C≡CPh. Similar trends were observed for the long-wavelength UV-vis absorption and photoluminescence properties. The emission maxima range from 605 to 675 nm at 298 K in CH₂Cl₂ solution and from 555 to 655 nm at 77 K in glassy frozen CH₂Cl₂/MeOH matrices. Large differences in amplitude-weighted average lifetimes τ_{av} (up to 0.9 µs at 298 K, up to 12 µs at 77 K) and photoluminescence quantum yields Φ_L (up to 0.15 at 298 K and up to 0.82 at 77 K) were found. TD-DFT calculations showed that the decomposition of the triplet excited states into LC (π−π*, centred in the individual parts of the C^N^N ligand) and LLCT (π−π*, between the individual parts of the C^N^N ligand + X−π* from coligand to C^N^N) contributions for the ligand-centred states as well as MLCT (d_{Pt}-to-$\pi^*_{C^N^N}$) and LMCT (p_{Cl} or π_{CCR}-to-d_{Pt}) character for the charge-transfer states involving the metal is beneficial to assess the participation of the individual heteroaryl groups of the C^N^N ligands. In view of the modular synthesis of these ligands, this will allow the realisation of tailor-made Pt(ɪɪ) triplet emitters in future work.

[a]Universität zu Köln, Department für Chemie, Institut für Anorganische Chemie, Greinstraße 6, D-50939 Köln, Germany. E-mail: krause.maren@gmx.net, jfried20@uni-koeln.de, annemarie.berger@uni-koeln.de, simonmartin.schmitz@gmail.com, axel.klein@uni-koeln.de
[b]Westfälische Wilhelms-Universität Münster, Institut für Anorganische und Analytische Chemie, CiMIC, CeNTech, Heisenbergstraße 11, D-48149 Münster, Germany. E-mail: s_buss14@uni-muenster.de, cstra_01@uni-muenster.de
[c]Westfälische Wilhelms-Universität Münster, Institut für Festkörpertheorie und Center for Multiscale Theory and Computation, Wilhelm-Klemm-Straße 10, 48149 Münster, Germany. E-mail: dana.bruenink@googlemail.com, nikos.doltsinis@wwu.de

Introduction

The interesting cyclometalated Pt(ɪɪ) complexes as triplet emitters have been recognised and developed by rational design in recent years for applications in luminescent materials and for biological applications.[1–20] The d⁸-configured metal ion in combination with π-accepting ligands (low lying π* orbitals) provides long-lived metal-to-ligand charge transfer (MLCT) excited states whereas heteroaromatic ligands allow the admixture of π–π* (IL) configurations to yield mixed MLCT/IL excited states.[1–22] The so-called 'dark' d–d* states, as their population leads to rapid radiationless decay of excited molecules, can be suppressed through rigidity of both the organic ligand and the square planar coordination along with a strong ligand field.[5,10,12,15–17,22–27] Thus, bidentate,[1,3–8,13,14,16–18,20–22] tridentate,[1,6–8,10,13,15–20,23–38] or tetradentate[1,2,6–9,11–13,16–18,31,39–41] cyclometalated heteroaromatic ligands have been frequently used.[1–28]

Amongst them, the tridentate variants C^N^N, N^C^N, and C^N^C require a fourth coligand (or ancillary ligand) to com-

plete the square planar coordination environment. The fourth coordination site is frequently considered to be prone to distortion and thus enhancing radiationless decay. Recent work has shown that careful choice of these coligands allows for fine-tuning of the triplet emission properties, as high quantum yields and long lifetime have been reported.[1,15,17,25,31,34,36] For the optimisation of the photoluminescence properties of such complexes, combined experimental and theoretical studies are helpful.[5,6,8,9,12,15,18,21,23–28] Variation of these ligands, including substitution of the heteroaromatic units has previously allowed the generation of complexes with photoluminescence (PL) quantum yields Φ_L of up to 100% and a broad range of emission energies.[1,2,6,8–17,20,24,27,31,34] Unfortunately, in many cases, structurally very similar derivatives of these complexes failed to perform in the same way and the reasons remained unclear.[31] DFT modelling has allowed emission energies to be rationalised; however, quantum yields are less predictable.[4,9,10,12,15,24,26,29,41,42] Very recently, DFT calculations have started to seek quantitative insight into the character and dynamic behaviour of the excited states of transition metal complexes,[12,21,41–46] also allowing the rationalisation of differences in quantum yields.

A prominent example where structurally very similar complexes show very different luminescence efficiencies was recently published by Che *et al.*[31] reporting on [Pt(C^N^N)X] (X = Cl or C≡C$_6$F$_5$) complexes (Scheme 1, **A**) with cyclometalating C^N^N ligands in which the **C aryl** unit included various substituted phenyl (R-ph), naphthyl (na), thiophenyl (th), or benzothiophenyl (bth) groups, whereas the **central N** unit involved always the 4-(3,5-di-*tert*-butyl-phenyl)pyridyl (tbppy) group and the **peripheral N** group pyridyl (py), 1-quinolinyl (1-quin), 2-quinolinyl (2-quin) or 3-isoquinolinyl (3-isoquin). In this series of complexes, the efficiency expressed by Φ_L varied from <0.001 to 0.99 (thus almost unity) in CH$_2$Cl$_2$ at 298 K.[31] This extended an earlier study by Che *et al.* on complexes replacing the **C aryl** group by R-ph, na and th, a central 4-(4-carboxy)phenyl-pyridyl group and a peripheral pyridyl unit (Scheme 1, **B**). These complexes achieved Φ_L of only 0.002 to 0.01, while the N^C^N derivative (**N** = py, **C** = 4(4-carboxy) phenyl-phenyl) showed a Φ_L of 0.44 in CHCl$_3$.[32] Very recently Huo *et al.* reported series of [Pt(C^N^N)X] (X = Cl, C≡CPh, or Ph) containing a pyrazolyl (pz) **peripheral N** group, a pyridyl **central N** group and various **C aryl** groups including R-ph, na, th, and bth (Scheme 1, **C**).[30] As in the case of the recent work by Che *et al.*,[31] the Φ_L at 298 K in this extensive work ranged from <0.0001 to 0.62 with [Pt(ph(py)pz)C≡CPh] being the most potent derivative within this extensive study.

Although there is now a rich body of experimental data available, no obvious correlation between the individual **C** and **N** units and high Φ_L or other desirable photoluminescence properties has emerged. The recent work by Che *et al.* provided limited insights into the excited states through (TD)-DFT calculations on two selected complexes.[31] The authors attribute the vast differences in the luminescence properties to different contributions to the emission from ^{3}MLCT (d$_{Pt}$-to-$\pi^*_{C^N^N}$), $^3\pi$–π^*, and XLCT (p$_{Cl}$-to-π^*) excited states for the chlorido com-
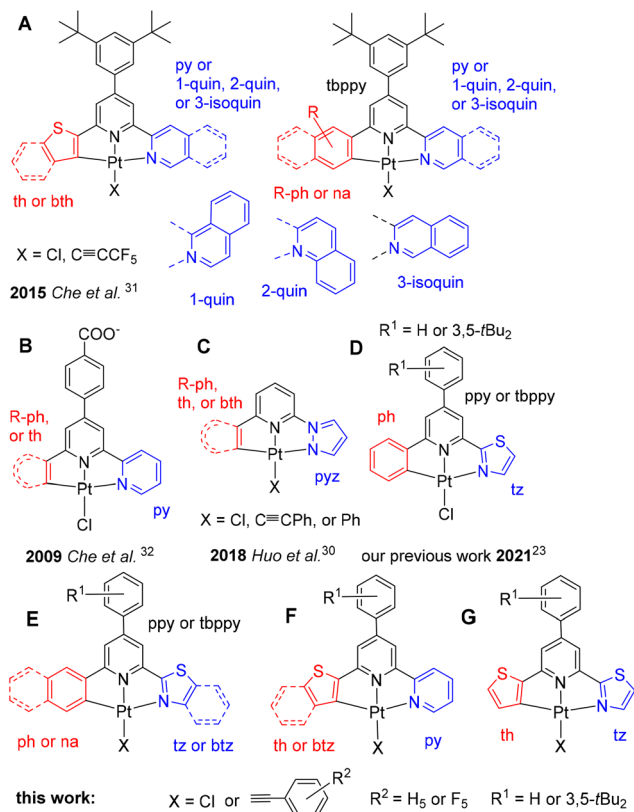
Scheme 1 Structures of previously reported complexes [Pt(C^N^N)X] (**A** to **D**),[23,30–32] and those under study (**E** to **G**) (th = thiophenyl, bth = benzothiophenyl, py = pyridyl, 1-quin = 1- quinolinyl, 2-quin = 2-quinolinyl, 3-isoquin = 3-isoquinolinyl, R-ph = substituted phenyl, na = naphthyl, pyz = pyridazolyl, tz = thiazolyl, btz = benzothiazolyl.

plexes and ^{3}MLCT, $^3\pi$–π^* and ^{3}L′LCT ($\pi_{C≡C}$–π^*) for the alkynyl derivatives,[31] following established ideas.[39,47] In a subsequent DFT study, the benchmarking complex [Pt(ph(tbppy)3-isoquin) (C≡CC$_6$F$_5$)] (Φ_L = 0.99 at 298 K in solution) was compared to the three derivatives containing na (instead of ph), py (instead of 3-isoquin), and Cl (instead of C≡CC$_6$F$_5$).[43] When breaking down the contributions to the excited triplet T$_1$ state, the calculations showed a remarkably high participation of the Pt d$_{xz}$ orbital to the highest occupied molecular orbital (HOMO) for the parent complex alongside with a high contribution of the C≡CC$_6$F$_5$ moiety; thus a high ^{3}MLCT and ^{3}L′LCT character of the triplet excited state can be assessed. Further, the S$_1$ and S$_2$ states are composed of two effective excitations, namely HOMO−1 → LUMO and HOMO → LUMO resulting in the largest radiative rate constant k_r in this series of complexes. Further, the energy barrier between the ^{3}MC and the T$_1$ is high for the parent complex and the non-radiative rate constant k_{nr} very small. The same is basically true for the Cl derivative, but not for the na and py derivatives,[43] which matches qualitatively well the observed rate-constants and Φ_L.[31]

We recently studied the electronic states of the Pt(C^N^N) complexes [Pt(ph(tbppy)tz)Cl] and [Pt(ph(py)tz)Cl] alongside with their corresponding Pd(II) derivatives using a variety of

Table 1 Summary of the complexes [Pt(C^N^N)X] in this study[a]

No.	Class[b]	[Pt(C^N^N)X]	C_{aryl}	$N_{central}$	$N_{peripheral}$	Coligand
1	**A**	[Pt(ph(ppy)tz)Cl][23]	ph	ppy (R^1 = H)	tz	Cl
2		[Pt(ph(tbppy)tz)Cl][23]	ph	tbppy (R^1 = 3,5-tBu$_2$)	tz	Cl
3		[Pt(ph(tbppy)tz)(CCPh)]	ph	tbppy (R^1 = 3,5-tBu$_2$)	tz	C≡CPh
4		[Pt(ph(tbppy)tz)(CCC$_6$F$_5$)]	ph	tbppy (R^1 = 3,5-tBu$_2$)	tz	C≡CC$_6$F$_5$
5		[Pt(na(tbppy)tz)Cl]	na	tbppy (R^1 = 3,5-tBu$_2$)	tz	Cl
6		[Pt(na(tbppy)tz)(CCPh)]	na	tbppy (R^1 = 3,5-tBu$_2$)	tz	C≡CPh
7		[Pt(ph(ppy)btz)Cl]	ph	ppy (R^1 = H)	btz	Cl
8		[Pt(ph(tbppy)btz)Cl]	ph	tbppy (R^1 = 3,5-tBu$_2$)	btz	Cl
9		[Pt(ph(tbppy)btz)(CCPh)]	ph	tbppy (R^1 = 3,5-tBu$_2$)	btz	C≡CPh
10	**B**	[Pt(th(ppy)py)Cl]	th	ppy (R^1 = H)	py	Cl
11		[Pt(th(tbppy)py)Cl]	th	tbppy (R^1 = 3,5-tBu$_2$)	py	Cl
12		[Pt(th(tbppy)py)(CCPh)]	th	tbppy (R^1 = 3,5-tBu$_2$)	py	C≡CPh
13		[Pt(th(tbppy)py)(CCC$_6$F$_5$)]	th	tbppy (R^1 = 3,5-tBu$_2$)	py	C≡CC$_6$F$_5$
14		[Pt(bth(ppy)py)Cl]	bth	ppy (R^1 = H)	py	Cl
15		[Pt(bth(tbppy)py)Cl]	bth	tbppy (R^1 = 3,5-tBu$_2$)	py	Cl
16		[Pt(bth(tbppy)py)(CCPh)]	bth	tbppy (R^1 = 3,5-tBu$_2$)	py	C≡CPh
17	**C**	[Pt(th(tbppy)tz)Cl]	th	tbppy (R^1 = 3,5-tBu$_2$)	tz	Cl
18		[Pt(th(tbppy)tz)(CCPh)]	th	tbppy (R^1 = 3,5-tBu$_2$)	tz	C≡CPh

[a] See Scheme 1; phenyl (ph)/naphthyl (na)/thiophenyl (th)/benzothiophenyl (bth), 4-phenyl-pyridyl (ppy)/3,5-tBu$_2$-phenyl-pyridyl (tbppy), pyridyl (py)/thiazolyl (tz)/benzothiazolyl (btz). [b] Classes of complexes defined for the discussion.

DFT-based tools (Scheme 1, **D**).[23] This motivated us to apply these methods also to the excited states properties and dynamics on a broader series of [Pt(C^N^N)X] complexes, and we herein report a series of Pt(II) complexes [Pt(C^N^N)X] with the coligands X = Cl, C≡CPh, C≡CC$_6$F$_5$ as well as cyclometalating tridentate C^N^N ligands based on 2-(6-arylpyridin-2-yl)thiazoles and 2-(6-arylpyridin-2-yl)thiophenes (Scheme 1 **E** to **G** and Table 1). We have synthesised 16 new complexes and studied experimentally their electrochemical and photophysical properties in detail. The **C aryl** group was varied using phenyl (ph), naphthyl (na), thiophenyl (th), or benzothiophenyl (bth). Phenylpyridine (ppy) or its 3,5-di-*tert*-butyl derivative (tbppy) represent the **central N** core and the **peripheral N** group was varied using pyridyl (py), thiazolyl (tz), or benzothiazolyl (btz). Although they contain different groups, they form pairs of formally isoelectronic complexes, *e.g.* [Pt(ph(ppy)tz)X] and [Pt(th(ppy)py)X], as the thiazolyl and thiophenyl as well as the phenyl and pyridyl groups are isoelectronic. The central phenylpyridyl unit had turned out to be beneficial for the ability of such cyclometalated complex to act as efficient triplet emitters.[10,31–34,36,41] For the variation of the coligand X, we expected to increase the ligand-field splitting (LFS) when going from the Cl coligand to phenylacetylido (C≡CPh) and pentaflourophenylacetylido (C≡CC$_6$F$_5$) ligands. The stronger σ-donor character of these organic ligands destabilises the otherwise thermally accessible MC-states towards improved emission efficiencies.[1,17,30–32,34,36]

As in our previous study,[23] we calculated UV-vis absorption and emission spectra using (TD)-DFT methods and decomposed the triplet emitting states into LC (π–π*, centred in the individual parts of the C^N^N ligand), LLCT (π–π*, between the individual parts of the C^N^N ligand and X–π*, between the coligand and the C^N^N), MLCT (d$_{Pt}$-to-π*$_{C^N^N}$), and

LMCT (p$_{Cl}$ or π$_{CCR}$-to-d$_{Pt}$) contributions. The decomposition of ligand-centred states into LC and LLCT character goes beyond previous DFT analyses of such complexes[31,42–44] and turned out very helpful to assess adequately the contributions of the individual heteroaryl groups of the C^N^N ligands.

Results and discussion

Synthesis and characterisation

The HC^N^N protoligands (ligand precursors prior to cyclometalation) were assembled from the corresponding chalcones using the versatile Kröhnke synthesis (further details are found in the ESI†). The Pt(II) chlorido complexes were synthesised from the HC^N^N protoligands and K$_2$[PtCl$_4$] with up to 98% yield as orange to red solids. For excellent yields, a sufficient stirring and long reaction times with up to 3 days are required. The chlorido coligand was exchanged for alkynides under Sonogashira-like conditions in yields ranging from 69 to 96%. The compounds were analysed and characterised through elemental analysis, ^{1}H NMR spectroscopy, and EI-MS (+) or HR-ESI-MS(+) (see Experimental section in the ESI†). The solubility of most of the complexes in common organic solvents is generally low but is significantly increased by decoration of the phenylpyridine with *tert*-butyl groups.

Crystal and molecular structures

The two compounds [Pt(ph(tbppy)btz)(C≡CPh)] (**9**) and [Pt(th(ppy)py)Cl]·CD$_2$Cl$_2$ (**10**·CH$_2$Cl$_2$) were obtained as single crystals. Their crystal and molecular structures were studied by X-ray diffractometry experiments. Details of the structure solution and refinement (Table S1, ESI†) as well as figures showing the crystal structures (Fig. S1 to S4, ESI†) can be found in the ESI.† Both
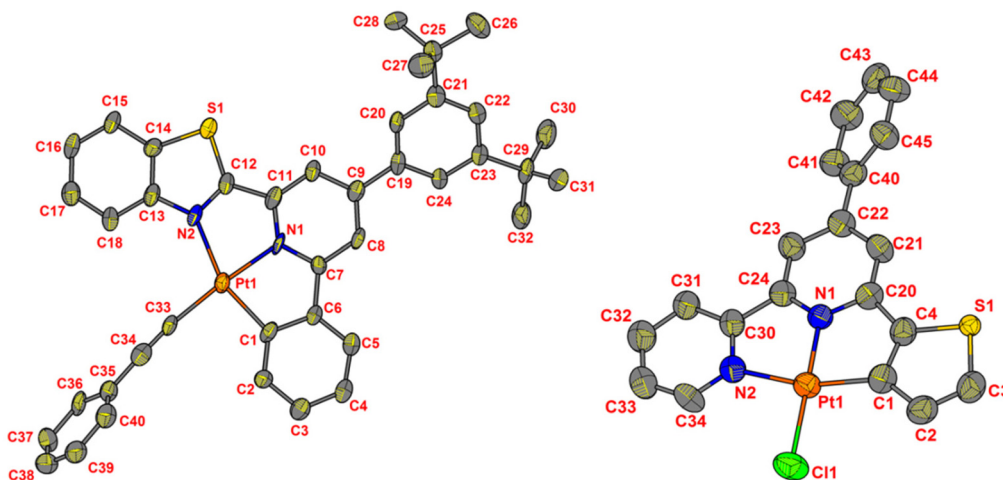
Fig. 1 ORTEP plot of the Pt(ıı) complex in [Pt(ph(tbppy)btz)(C≡CPh)] (**9**) (left) and [Pt(th(ppy)py)Cl]·CH$_2$Cl$_2$ (**10**·CH$_2$Cl$_2$) (right) with ellipsoids at 50% probability. Co-crystallised CD$_2$Cl$_2$ and H atoms were omitted for clarity.

complexes show intermolecular π-stacking interactions with short centroid···centroid distances around 3.5 Å (Fig. S4†), which is characteristic for such complexes.[10,13,15,24–28,30,31,33]

Both complexes show planar geometries around the Pt atoms and almost planar C^N^N ligand cores (Fig. 1). The pending phenyl or di-*tert*-butyl-phenyl groups appear twisted towards this plane. Also, the phenyl group of the C≡CPh ligand in **9** shows a deviation of 65.8(3)° from the coordination plane (data in Table S2†).

Electrochemistry and DFT-calculated frontier orbitals of the complexes

The complexes showed a first reversible one-electron reduction wave in the range from −1.5 to −1.8 V (Fig. 2 and 3, Fig. S5 to S22, Table S4†). The first wave is usually followed by a second fully or partly reversible reduction wave at very low potentials (−2.1 to −2.5 V). A similar behaviour is observed for the proto-ligands HC^N^N at potentials lying about 0.8 V lower than those corresponding to the complexes (Fig. S23 to S26 and Table S3†).

The reduction potentials are very similar for the (benzo) thiophenyl complexes having an opposite thiazolyl moiety

(Fig. 3A) and they are approximately invariant for the progression phenyl – naphthyl – thiophenyl (Fig. 3B). For the variation of the **peripheral N** group, the potentials increase along the series pyridine < thiazolyl < benzothiazolyl (Fig. 3B), while variation of the **central N** unit from ppy to tbppy leads only to subtle changes. Exchange of the coligand has almost no influence on the reduction potentials. We thus assign the first reductions as essentially taking place at the bipyridine and pyridyl(thiazolyl) moieties, in line with results for comparable complexes,[10,13,23,24,33,35,48–57] with DFT calculated lowest unoccupied molecular orbitals (LUMO) for the phenyl complexes [Pt(ph(ppy)tz)Cl] (**1**) and [Pt(ph(tbppy)tz)Cl] (**2**),[23] and calculations on the thiophenyl derivatives [Pt(th(tbppy)py)Cl] (**11**) and [Pt(th(tbppy)py)(C≡CPh)] (**12**) (Fig. S29†). The second reduction waves are separated by about 0.6 to 0.7 V, indicating that the second reduction events are also ligand-centred and a Pt^{II} → Pt^{I} reduction being unlikely.

On the anodic side, irreversible and in part poorly defined first oxidation waves are recorded in the range 0.1 to 0.9 V. Potentials for comparable Cl and C≡CC$_6$F$_5$ complexes are very similar; complexes with C≡CPh show a cathodic shift in agreement with a stronger σ donor ability of C≡CPh compared with Cl. In the case of fluoro substituents in C≡CC$_6$F$_5$, the σ donor ability is decreased making its overall impact on the electron density comparable to Cl. Very different oxidation potentials were found for variations in the **C aryl** group. Within the series of Cl complexes possesing a central tbppy unit, the potentials increase along the series bth < ph < th (Fig. 3A); however, for the oxidation waves, also the central py, ppy, or tbppy units seem to be of importance and a simple correlation is not obvious. The same is true for the complexes containing C≡CPh coligands, where all three groups seem to contribute, as indicated by the very different potentials for the two complexes containing the ph (tbppy)tz and ph(tbppy)btz ligand (Fig. 3B). Reports for similar complexes suggest essentially metal (Pt^{II}/Pt^{III}) based oxidation processes.[2,10,13,23,24,33,48–57] Our results agree with this hypothesis
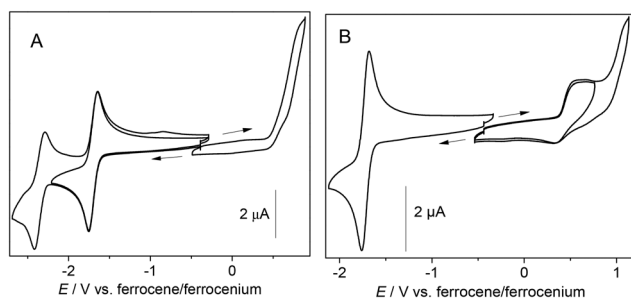

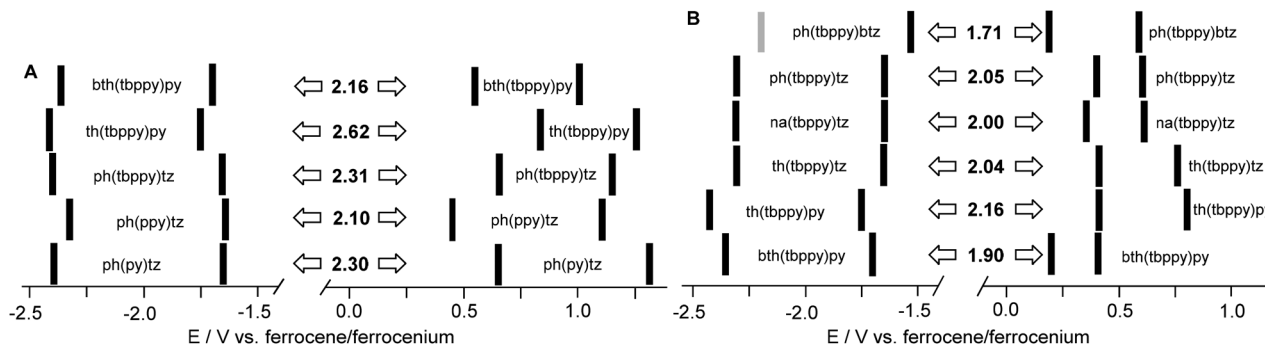**Fig. 2** Cyclic voltammograms of [Pt(bth(tbppy)py)Cl] (**15**) in 0.1 M *n*Bu$_4$NPF$_6$/THF (A) and /CH$_2$Cl$_2$ (B).

Fig. 3 Redox potentials of [Pt(C^N^N)Cl] (A) and [Pt(C^N^N)C≡CPh] (B) complexes. The bars represent the experimental potentials (see Table S4, ESI†).

but also show strong contributions from the coligand and the *C* **aryl** group.

Our series of complexes covers a vast range of electrochemical gaps from 1.7 to 2.6 eV (Fig. 3, Table S4, ESI†) between the first reductions ranging from about −1.5 to −1.8 V and the first oxidations ranging from about 0.1 to 0.9 V. Thus, the gaps are essentially governed by the oxidation potentials. The smallest gaps were found for [Pt(ph(tbppy)btz)C≡CPh] (**9**) (1.71 eV) and [Pt(bth(tbppy)py)C≡CPh] (**16**) (1.90 eV) which are complexes bearing the same coligand but structurally very different, although isoelectronic, C^N^N ligands. The largest gaps were those of the th(tbppy)py (**11**) (2.62 eV) and ph(tbppy)tz (**2**) (2.31 V) complexes with the Cl coligand, which are also very different but isoelectronic. The similarity of the gaps for both pairs of complexes is probably the result of several electron-donating and -accepting effects compensating each other.

Experimental and TD-DFT calculated UV-vis absorption spectra

At a first glance, all complexes show similar absorption spectra with structured and intense bands in the range 250 to 400 nm, along with a partially structured band system from 400 to 500 nm with medium intensity and weak absorption bands in the 500 to 600 nm range (Fig. 4 and 5 and S31 to S44;† selected data in Table 2, full data in Table S6†). The intense UV bands appear also for the protoligands HC^N^N (Fig. S30, Table S5†) and can thus be assigned to transitions into states with predominant π–π* character.

With the exception of complexes **5**, **7**, **8**, **14**, and **15**, all structures were optimised in the electronic ground state using DFT (for images, see Fig. S28 and S29†). The theoretical structures match very well with the experimentally obtained geometries for the complexes **9** and **10** and other derivatives. Based on these geometries, UV-vis absorption spectra were calculated using TD-DFT and compared with the experimental spectra. Fig. 4 compares all complexes carrying the C≡CPh coligand and shows a good match between calculated and experimental data in the UV range spanning from 200 to 350 nm, while for the visible range (350 to 500 nm) the calculated long-wavelength bands were slightly blue-shifted compared with the

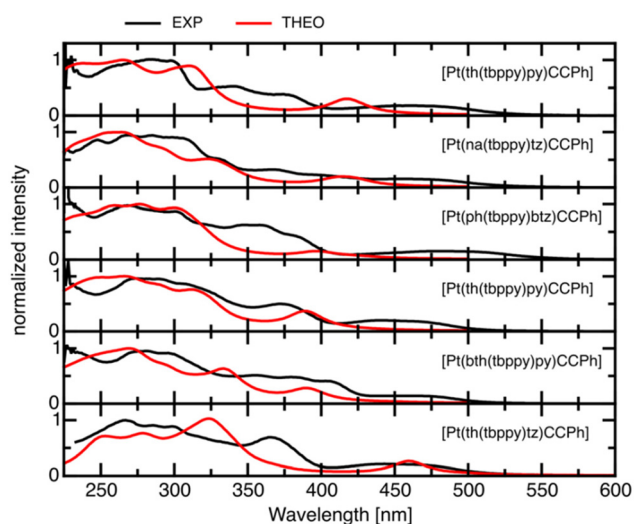**Fig. 4** TD-DFT-calculated UV-vis absorption spectra (THEO, red) compared to experimental spectra (EXP, black) for all complexes with the C≡CPh coligand.

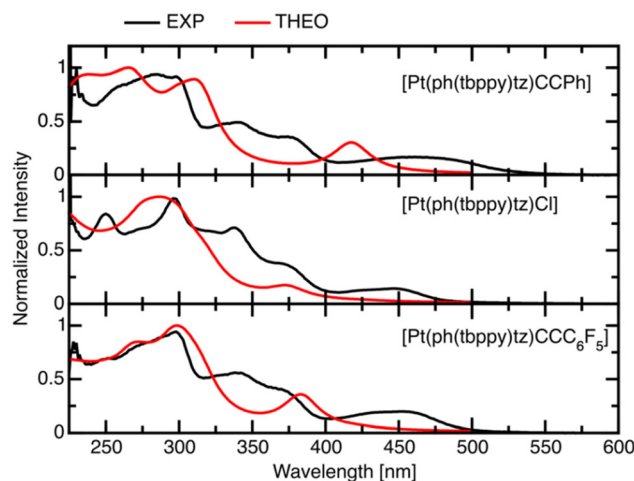**Fig. 5** TD-DFT calculated UV-vis absorption spectra (THEO, red) of compared to experimental spectra (EXP, black) of [Pt(ph(tbppy)tz)C≡CPh] (**3**), [Pt(ph(tbppy)tz)Cl] (**2**), and [Pt(ph(tbppy)tz)C≡CC₆F₅] (**4**).

Table 2 Selected experimental photophysical data for the [Pt(C^N^N)X] complexes

Complex	T^a/K	$\lambda_{abs}{}^b$ /nm	$\lambda_{em}{}^c$/nm	$\tau_{av}{}^d$ /µs	$\Phi_L \pm 0.02/\pm 0.05^e$	k_R/10^5 s$^{-1\,f}$	k_{NR}/10^5 s$^{-1\,g}$
A [Pt(ph(tbppy)tz)Cl] (**2**)^h	298	301, 340, 370, 446	608	0.71	0.07	1.0 ± 0.3	13.0 ± 0.4
	77	300, 333, 360, 429	557, 603, 662sh	4.01	0.22	0.55 ± 0.14	2.0 ± 0.2
[Pt(ph(tbppy)tz)C≡CPh] (**3**)	298	302, 346, 380, 443sh, 473, 495sh	626, 645sh	0.39	0.06	1.5 ± 0.7	24 ± 3
	77	336, 370, 425, 438, 468	558, 605, 660sh	3.50	0.62	1.8 ± 0.2	1.1 ± 0.3
[Pt(ph(tbppy)tz)C≡CC$_6$F$_5$] (**4**)	298	345, 370, 445sh, 465	605, 635sh	0.91	0.12	1.3 ± 0.3	9.7 ± 0.6
	77	340, 365, 420, 445	555, 600, 655sh, 725sh	3.53	0.49	1.39 ± 0.19	1.4 ± 0.3
[Pt(na(tbppy)tz)C≡CPh] (**6**)	298	311, 335sh, 370, 398, 420sh, 468	635	0.41	0.10	2.5 ± 0.6	22.1 ± 1.4
	77	330, 395, 437, 463	555, 595, (650sh)	3.97	0.82	2.1 ± 0.2	0.5 ± 0.3
[Pt(ph(tbppy)btz)Cl] (**8**)	298	353, 464	635, 675sh	0.21	< 0.02	≤ 2	47.6 ± 1.4
	77	346, 425, 452	600, 656, 710sh	1.59	0.07	0.4 ± 0.3	5.8 ± 0.6
[Pt(ph(tbppy)btz)C≡CPh] (**9**)	298	360, 470, 500sh	655	0.11	< 0.02	1.8 ± 1.8	87 ± 5
	77	360, 470, 500sh	600, 650, 700sh	1.70	0.18	1.1 ± 0.3	4.8 ± 0.5
B [Pt(th(tbppy)py)Cl] (**11**)	298	315, 370, 440	617, 660sh	1.81	0.07	≤ 0.4	9.6 ± 0.5
	77	375, 425, 470sh, 490sh	595, 645, 700	11.6	0.58	0.50 ± 0.08	0.36 ± 0.15
[Pt(th(tbppy)py)C≡CPh] (**12**)	298	300, 373, 440, 475sh	620, 660sh	1.63	0.14	0.86 ± 0.13	5.28 ± 0.17
	77	360, 425sh, 460	590, 640, 700sh	8.25	0.79	0.96 ± 0.10	0.25 ± 0.14
[Pt(th(tbppy)py)C≡CC$_6$F$_5$] (**13**)	298	312, 370, 425sh, 445	620, 660sh	2.18	0.15	0.7 ± 0.1	3.90 ± 0.13
	77	350–375, 430	595, 650, 705	8.7	0.79	0.91 ± 0.09	0.24 ± 0.13
[Pt(bth(tbppy)py)Cl] (**15**)	298	350, 395, 440sh	675, 730	1.07	0.03	0.28 ± 0.19	9.1 ± 0.3
	77	375, 480	655, 720, 745	4.16	0.13	0.31 ± 0.13	2.1 ± 0.2
[Pt(bth(tbppy)py)C≡CPh] (**16**)	298	360, 380sh, 405sh, 475	675, 740	1.11	0.04	0.36 ± 0.18	8.7 ± 0.3
	77	365, 400sh, 460	650, 720, 785	3.57	0.24	0.67 ± 0.16	2.1 ± 0.3
C [Pt(th(tbppy)tz)Cl] (**17**)	298	368, 450	655	0.22	<0.02	≤1.9	45 ± 3
	77	364, 430, 503sh	610, 660, 725sh	4.17	0.13	0.31 ± 0.13	2.1 ± 0.2
[Pt(th(tbppy)tz)C≡CPh] (**18**)	298	375, 470	658	0.25	<0.02	≤1.6	39.6 ± 1.1
	77	365, 425, 454	604, 657, 725sh	4.19	0.35	0.84 ± 0.15	1.6 ± 0.2

^{a} Ar-Purged CH$_2$Cl$_2$ solution at 298 K or frozen glassy matrix of CH$_2$Cl$_2$/MeOH (1 : 1) at 77 K. ^{b} Absorption data including molar absorption coefficients in Table S6, ESI.† ^{c} λ_{exc} = 350 nm, sh = shoulder. ^{d} λ_{exc} = 376 nm, amplitude-weighted average lifetime (the single exponential components and relative amplitudes are listed in Table S7†), the corresponding uncertainties are found in the ESI.† ^{e} The uncertainties for the glassy matrices are higher due to the measurement set up. ^{f} Average radiative deactivation rate constants from the amplitude-weighted average lifetimes and their uncertainties are calculated as follows: $k_R = \dfrac{\Phi_L}{\tau_{av}}$; $\Delta k_R = \left(\dfrac{\Delta \Phi_L}{\tau_{av}}\right) + \left(\dfrac{\Delta \tau_{av}}{\tau_{av}{}^2} \cdot \Phi_L\right)$.[59] ^{g} Average radiationless deactivation rate constants from the amplitude-weighted average lifetimes and their uncertainties are calculated as follows: $k_{NR} = \dfrac{1 - \Phi_L}{\tau_{av}}$; $\Delta k_{NR} = \left(\dfrac{\Delta \tau_{av}}{\tau_{av}{}^2}\right) + \left(\dfrac{\Delta \Phi_L}{\tau_{av}}\right) + \left(\dfrac{\Delta \tau}{\tau_{av}{}^2} \cdot \Phi_L\right)$.[59] ^{h} From ref 23.

experimental bands. The weak transitions in the 500 to 600 nm range might thus be assigned to spin-forbidden absorption processes into the triplet manifold.

The long-wavelength absorption bands are markedly altered with the C^N^N variations, with maxima ranging from 435 to 505 nm. The change of coligands generally leads to red-shifts in the maxima along the series Cl < C≡CC$_6$F$_5$ < C≡CPh (Fig. 5, Fig. S36 and S40†) in agreement with the influence of the electron-withdrawing F substituents, whereas the Cl complexes appear even further blue-shifted. This is fully in line with previous reports.[31,43,57,58] The highest energies for these absorption bands were found for the th(tbppy)py (**11**) and th(tbppy)tz (**17**) (436 nm) complexes bearing the Cl ligand. By far, the lowest energy was recorded at 505 nm for [Pt(ph(tbppy)btz)C≡CPh] (**9**), which obviously combines preferential **C aryl** and **peripheral N** groups for a low-energy absorption. However, the four "second-best" candidates [Pt(bth(tbppy)py)C≡CPh] (**16**) (469 nm), [Pt(th(tbppy)tz)C≡CPh] (**18**) (468 nm), [Pt(ph(tbppy)tz)C≡CPh] (**3**) (466 nm), and [Pt(ph(tbppy)btz)Cl] (**8**) (466 nm) are structurally very dissimilar, but their com-

parable energies might be the result of several effects and a best combination of **C aryl** and **peripheral N** groups cannot be deduced.

Experimental photoluminescence spectra

The photoluminescence (PL) spectra of all complexes (Fig. 6, and Fig. S37 to S106†) are characterised by broad emission bands at 298 K which partially gain vibrational structure upon cooling to 77 K. The PL properties are summarised in Table 2 (for the complete set of data with the uncertainties as well as the multiexponential decay components, see Fig. S54 to S106 and Table S7†). The excitation spectra (data in Table 2) mirror their absorption counterparts (Table S6†).

The change from the central ppy to tbppy has a marginal influence on the emissive properties of the complexes, in line with our recent report on [Pt(ph(ppy)py)Cl] (**1**) and [Pt(ph(tbppy)py)Cl] (**2**).[23] However, the superior solubility of the tbppy was remarkable and we focused on these derivatives for the photophysical measurements, thus omitting complexes **1**, **10** and **14** in Table 2. Also very generally, in CH$_2$Cl$_2$ solutions
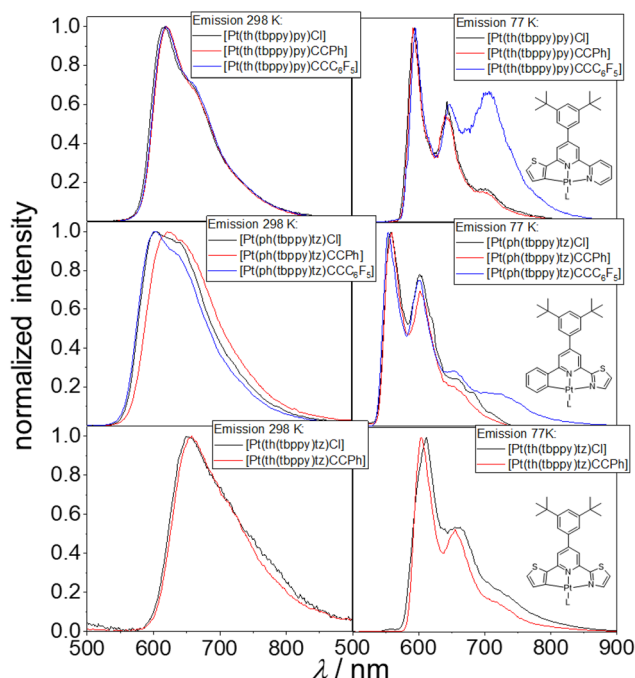
Fig. 6 Normalised photoluminescence spectra (λ_{exc} = 350 nm) of all classes of complexes with focus on the influence of the co-ligand; top = **class A**: [Pt(ph(tbppy)tz)Cl] (**2**) (black), [Pt(ph(tbppy)tz)C≡CPh] (**3**) (red) and [Pt(ph(tbppy)tz)C≡CC₆F₅] (**4**) (blue); centre = **class B**: [Pt(th(tbppy)py)Cl] (**11**) (black), [Pt(th(tbppy)py)C≡CPh] (**12**) (red) and [Pt(th(tbppy)py)C≡CC₆F₅] (**13**) (blue); bottom = **class C**: [Pt(th(tbppy)tz)Cl] (**17**) (black) and [Pt(th(tbppy)tz)C≡CPh] (**18**) (red). Measured in Ar-purged CH_2Cl_2 at 298 K (left) or frozen glassy CH_2Cl_2/MeOH matrices at 77 K (right).

at 298 K, the triplet states are quenched by dissolved O_2, as evidenced by the τ_{av} and Φ_L values, which are increased upon purging with argon (see also Table S7†).

The complex [Pt(ph(tbppy)tz)Cl] (**2**) benchmarks the **class A** (Table 2) of complexes containing a peripheral phenyl (ph) or naphthyl (na) **C aryl** group as well as a **peripheral N** (benzo) thiazolyl, and shows a broad emission peaking at λ_{max} = 608 nm (Fig. 6) with an incipient vibronic progression and amplitude-averaged lifetime τ_{av} of 0.714 µs with a photoluminescence quantum yield of Φ_L = 0.07 at 298 K. The quantum yield is markedly increased for the C≡CC₆F₅ derivative **4** (600 nm, 3.53 µs, Φ_L = 0.12) and also slightly for the naphthyl complex [Pt(na(tbppy)tz)C≡CPh] (**6**) (595 nm, 3.97 µs, Φ_L = 0.10). Counterintuitively and probably due to additional rotovibrational modes, the non-radiative rate constant k_{NR} at 298 K is increased from ~13 × 10⁵ s⁻¹ to ~24 × 10⁵ s⁻¹ when going from Cl to C≡CPh (**2** → **3**, **5** → **6**, **8** → **9**) and dropped when going to C≡CC₆F₅ (~10 × 10⁵ s⁻¹, **4**); however, the radiative rate constants k_R are increased for both types of alkynyl complexes. The marked red-shifts of the emission maxima when introducing benzothiazolyl (**1** → **7**) instead of thiazolyl (**2** → **8**) (Fig. S44†) goes along with a reduction of Φ_L, which seems to be mainly caused by the markedly increased k_{NR} values, while the k_R values drop only slightly. This can be

attributed to the energy-gap law (EGL). In contrast, the change from phenyl to naphthyl (**3** → **6**) has almost no impact on the spectra, but markedly increases the Φ_L. In frozen glassy matrices (CH_2Cl_2 : MeOH; 1 : 1) at 77 K, the quantum yields are generally higher. Here, starting from **2** (Φ = 0.22), variation of ph to na or from Cl to C≡CPh allowed us to increase the quantum yield up to a Φ_L of 0.82 (**6**), thus matching the highest values from the previous studies.[30–32]

For [Pt(th(tbppy)py)Cl] (**11**), as a starting point for **class B** (Table 2), for the complexes that contain a (benzo)thiophenyl **C unit** and a pyridine **peripheral N** group, a vibronic progression is visible but not completely pronounced with λ_{max} = 617 nm, τ_{av} = 1.809 µs and Φ_L = 0.07 at 298 K (Fig. 6), which is similar to the benchmark from **class A**, the complex [Pt(ph(tbppy)tz)Cl] (**2**). Both complexes constitute structural isomers in view of their atoms and their ring systems, but the variation of ph vs. th and tz vs. py might strongly affect the HOMO and the LUMO energies as well as the photoluminescence properties (the reasons will be discussed in the DFT-section, *vide infra*).

Thus, this similarity represents probably a cancellation of several effects. The markedly different behaviour at 77 K with a much larger Φ_L for the thiophenyl (th) complex **17** (**class C**) points into this direction. As in **class A** complexes, going from thiophenyl (**10** → **13**) to the corresponding benzothiophenyl (**14** → **16**) derivatives leads to a red shift (Fig. S39†). For **class B** complexes, this has a stronger impact than the change tz → btz and we assume a higher $^3\pi$–π^* character of the excited state for the (b)th complexes in line with the more pronounced vibronic progression. The τ_{av}, as well as the Φ_L dropped (τ_{av} = 1.809 µs/Φ_L = 0.07 to τ_{av} = 1.069 µs/Φ_L = 0.03 in the case of [Pt(R(tbppy)py)Cl] (R = bth (**15**) vs. th (**11**)), most likely due to the energy-gap law leading to faster radiationless decays with increased k_{NR}-values. An interesting exception is the naphthyl complex [Pt(na(tbppy)tz)C≡CPh] (**6**). When compared to the ph analogue **3**, a smaller red shift at 298 K along with a higher k_R is found, whereas at 77 K the emission appears very slightly blue shifted with a higher Φ_L (0.82 vs. 0.62).

When going from fluid CH_2Cl_2 at 298 K to frozen glassy CH_2Cl_2/MeOH matrices at 77 K, the emission spectra show a pronounced vibronic progression and extended lifetimes. This can be attributed to the loss of solvent stabilisation. Nonetheless, the k_R values remain essentially unaffected, whereas for the complexes displaying a bigger impact, the values remain in the same order of magnitude. The k_{NR}-values, on the other hand, are all dramatically decreased due to the suppression of otherwise thermally accessible MC-mediated deactivation pathways.

Class C complexes combine the thiophenyl ring as a **C aryl** donor and a thiazolyl as the **peripheral N** donor in the tridentate ligand. In general, the broad yet unstructured emission maxima appear red-shifted to λ_{max} = 655 nm at 298 K, if compared with their extendend benzo-fused analogues while resembling **class B** complexes in this regard (Fig. S51†). However, upon cooling to 77 K, the properties are similar to **class A** derivatives. Besides a red-shift, the photophysical pro-

perties of [Pt(th(tbppy)tz)Cl] (**17**) at 298 K resemble those of [Pt(ph(tbppy)btz)Cl] (**8**); in frozen glassy matrices, the values are the same as for [Pt(bth(tbppy)py)Cl] (**15**) with a pronounced blue-shifted emission. The change of the coligand to yield [Pt(th(tbppy)tz)C≡CPh] (**18**) does not influence the emission wavelength, which resembles the behaviour of **class B** complexes. The overall values for [Pt(th(tbppy)tz)Cl] (**17**) can be best compared to [Pt(ph(tbppy)btz)C≡CPh] (**9**) at 298 K. So again, several effects compensate each other. Due to the loss of solvent stabilisation upon cooling (leading to more $^3\pi$–π*-character), the values at 77 K resemble again **class B** (*e.g.* [Pt(bth(tbppy)py)C≡CPh] (**16**)). All in all, **class C** complexes display photophysical properties lying between **classes A** and **B**, where at 298 K the MLCT-character is dominant, even though the coligand does not influence the emission maxima. In frozen glassy matrices, the loss of MLCT-character seems strong enough to resemble **class B**.

It is very interesting to compare our results with those reported for the very similar C^N^N-based Pt(II) complexes shown in Scheme 1 A (data in Table S8†).[31] As for our series, some of these complexes show relatively poor photoluminescene efficiency at 298 K with Φ_L reaching up to about 0.1 (such as in the case of [Pt(na(tbppy)py)Cl]), which fits perfectly into our series of structures. However, Table S8† shows derivatives with greatly enhanced Φ_L, which makes them worth describing (and comparing) more in detail. The introduction of 2-quinolinyl or 1-isoquinolinyl replacing the **peripheral N** pyridine unit (Scheme 1A) resulted in two complexes [Pt(ph(tbppy)2-quin) Cl] and [Pt(ph(tbppy)1-isoquin)Cl] with highly red-shifted emission profiles and low Φ_L (**class D** in Table S8†). In contrast to this, the introduction of the 3-isoquinolinyl group gave emitters with Φ_L up to 0.99 for (**class D**). As in our study, the introduction of the C≡CC$_6$F$_5$ coligand turned out to be beneficial in the benchmarking complex [Pt(ph(tbppy)3-isoquin) (C≡CC$_6$F$_5$)] (Φ_L = 0.99). At the same time, the emission of these complexes is markedly blue-shifted if compared with our derivatives containing **peripheral N** pyridyl or thiazolyl groups, which accounts at least for a part of the enhanced Φ_L (energy gap law). Interestingly, the variation of the **C aryl** phenyl group through substitution does not vary essentially the emission energy but markedly the Φ_L (from 0.14 to 0.79, **class E** in Table S8†). Introduction of thiophenyl instead of phenyl shifts the emission maxima closer to 600 nm (with high Φ_L); however, in the presence of benzothiophenyl (bth), the emission spectra are red-shifted to over 640 nm and the Φ_L values drop dramatically below 0.1 (**class F**). The authors explain these differences for two selected complexes invoking different contributions to the excited states, namely ^{3}MLCT (d-to-π* (C^N^N)), $^3\pi$–π*(C^N^N), and XLCT (p$_{Cl}$-to-π*(C^N^N)) for the chlorido complexes and ^{3}MLCT, $^3\pi$–π* and ^{3}L′LCT (π(CC-π* (C^N^N)) for the alkynyl derivatives.[31] The following TD-DFT-calculated emission spectra and their decomposition into different components for the excited triplet state (T$_1$) shed more light on these assumptions for our series of complexes.

When comparing the best candidates of previous studies with our series, the complexes **11**, **12**, and **13** evolve as strong

candidates with Φ_L of 0.60 and more at 77 K along with very long average lifetimes τ_{av} (~8–12 μs) at emission energies far lower than the benchmarking complex [Pt(ph(tbppy)3-isoquin) (C≡CC$_6$F$_5$)].[31] Taken the relatively low emission energy, the high Φ_L, and a long τ_{av} (876 μs), complex **13** is the most interesting candidate out of our series for applications, such as sensor arrays or optoelectronics, followed by complex **12** and **11**.

(TD)-DFT calculations on the excited states and emission spectra

Vibrationally resolved emission spectra from the T$_1$ state were calculated for selected complexes. In some cases, only the 0–0 transition energy (corrected for zero-point and thermal free energy contributions) could be computed due to numerical problems caused by insufficient overlap between the S$_0$ and T$_1$ wavefunctions. Fig. 7 shows a comparison of the calculated results at 300 K with the experimental emission spectra at 77 K and at RT for all complexes with the C≡CPh coligand. While the calculated curves match the experimental RT data quite well, they are considerably red-shifted compared to some of the experimental spectra at 77 K, in particular [Pt(ph(tbppy)tz) (C≡CPh)] (**3**) and [Pt(na(tbppy)tz)(C≡CPh)] (**6**).

Fig. S107† shows the influence of the central ligand (ppy *versus* tbppy) on the emission spectrum by comparing complexes [Pt(ph(ppy)tz)Cl] (**1**) and [Pt(ph(tbppy)tz)Cl] (**2**). As the calculated data confirm, the emission is affected very little by changing the central ligand from ppy to tbppy. When comparing the effect of different coligands (X = Cl, C≡CPh, and C≡CC$_6$F$_5$) on the emission spectra for [Pt(ph(tbppy)tz)X] complexes (Fig. S108†), the experimental spectra exhibit a very small blue-shift (less than 3 nm at 77 K) going from C≡CPh *via* Cl to C≡CC$_6$F$_5$, while the calculations produce a much
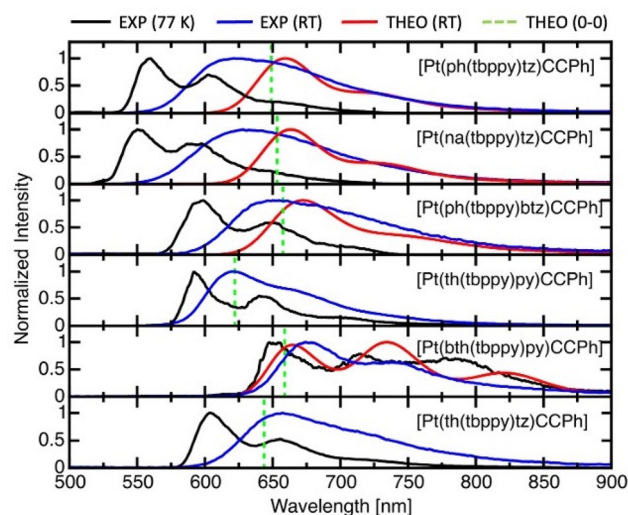

Fig. 7 DFT-calculated emission spectra (THEO, red) compared to experimental spectra (EXP) at 77 K (black) and RT (blue) for all complexes with the C≡CPh coligand. Calculated 0–0 transitions are shown as vertical dashed green lines.

more pronounced blue-shift, especially for $C \equiv CC_6F_5$. It is also worth noting that the calculated spectra of complexes **2** and **3** are in reasonable agreement with the experimental RT spectra, the experimental spectra at 77 K being considerably blue-shifted. For complex **4**, however, the calculated spectrum matches almost exactly the experimental data at 77 K. A very different picture emerges from a similar analysis for [Pt(th (tbppy)py)X] complexes (Fig. S109†). Here, the calculated spectra are practically unaffected by changing the coligand, which is in accord with the experimental data. Furthermore, there is a much smaller difference between the experimental spectra at 77 K and at RT, the latter being in very good agreement with the calculations.

To understand the reasons for the different behaviours of **class A** and **class B** compounds in the calculations, we analysed in detail the character of the respective $T_1 \rightarrow S_0$ transitions by performing a correlated electron–hole pair analysis.[60] Fig. S110 to S113† show the decomposition of the emissive T_1 states into the charge transfer contributions, namely MLCT (d_{Pt}-to-$\pi^*_{C^\wedge N^\wedge N}$) and LMCT ($p_{Cl}$ or π_{CCR}-to-d_{Pt}), as well as the ligand-centred excitations, namely LC (π–π^* in one of the components of the $C^\wedge N^\wedge N$ ligand) and LLCT (π–π^* between different components of the $C^\wedge N^\wedge N$ ligand), along with MC excitations possessing metal-centred character (d–d*). This goes beyond the previously presented decomposition into MLCT, π–π^*, and XLCT (for Cl as coligand or L'LCT (for the alkynyl derivatives),[29,31,36,42–44,47,57,58] and appears necessary in view of the individual contributions of the different parts of the $C^\wedge N^\wedge N$ ligand, as discussed above.

The charge-transfer character (both MLCT and LLCT) increases significantly when changing the **C aryl** group from ph to na (**3 → 6**). Going from ph to th (**3 → 18**), on the other hand, slightly decreases the MLCT contribution whilst significantly increasing the LLCT character (Fig. S110†). The comparison of **12** and **16** reveals that changing th for bth considerably reduces the MLCT participation. Introducing py as a **peripheral N** group instead of tz also decreases the overall CT contributions, therefore increasing the LC character (Fig. S110†).

The effect of the main ligand on the character of the emissive T_1 state is illustrated by comparing [Pt(ph(ppy)tz)Cl] (**1**) to [Pt(ph(tbppy)tz)Cl] (**2**) (Fig. S111†). Rather surprisingly, there are some sizable differences between the two compounds. Most notably, the MLCT character is higher for tbppy, while at the same time the LLCT contribution is lower. The analysis of the character of the emissive T_1 states and the influence of the coligand for **class A** complexes (Fig. S110 and S112†) shows that variations between the different coligands are small. The MLCT contribution is largest for Cl and smallest for $C \equiv CC_6F_5$, whereas the opposite is true for the LLCT character. An analogous analysis for **class B** derivatives (Fig. S113†) reveals that generally the LC contribution is considerably larger and the MLCT character much smaller than for **class A**, which could partially explain why the accuracy of the calculated emission spectra is seemingly higher for **class B** than for **class A** (Fig. S112 and S113†). Moreover, the influence of the coligand is smaller than in the case of **class A**.
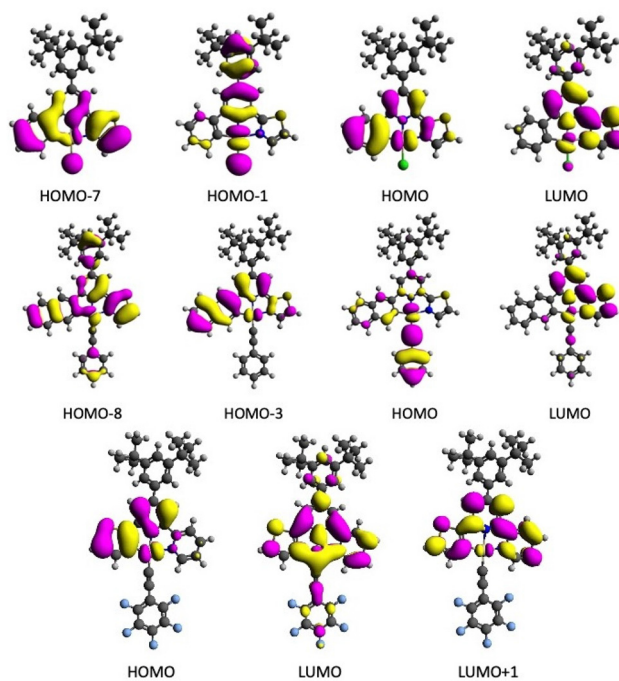

Fig. 8 Molecular orbitals of complexes **2** (top), **6** (middle) and **13** (bottom) with the largest contributions to the main monoelectronic excitations describing the emissive T_1 state.

In addition, we have determined for all calculated complexes (from the TD-DFT eigenvectors) which molecular orbitals make the largest contributions to the emissive T_1 states. All single-electron molecular orbital configurations that contribute at least 10% to the main configurations describing the emissive T_1 states are listed in Table S9.† Visualisations of all involved orbitals can be found in Fig. 8 and Fig. S114 to S121.† In none of the compounds, the emissive T_1 state corresponds to a pure HOMO–LUMO configuration; in some cases, other MO excitations are even more dominant. All contributing MOs have a pronounced metal component in addition to an extensive ligand part.

A closer look reveals, that extending the **C aryl** group from ph to na (Fig. 8) or from th to bth (Fig. S119 and S120†) fully extents the π system and thus HOMO components. The same is true for the extension of tz to btz (Fig. 8 and Fig. S117†). Both the Cl and the $C \equiv CPh$ coligands contribute exclusively to HOMO−n orbitals, including the HOMO for $C \equiv CPh$, while the $C \equiv CC_6F_5$ also contributes to the LUMO (Fig. 8) underpinning the special role of this coligand.[31,36,43,53,54,57,58]

Conclusions and outlook

Through a broad variation of the versatile cyclometalating anionic $^-C^\wedge N^\wedge N$ ligands and the ancillary ligands (or coligands) X in the Pt(II) complexes [Pt(C^N^N)X] (X = Cl, $C \equiv CPh$, or $C \equiv CC_6F_5$), we aimed to probe for the best combination of the potentially electron-donating peripheral **C aryl** group, the π accepting **peripheral N** group, and the coligand, while keeping

the **central N** core (4-(3,5-di-*tert*-butyl)phenyl)pyridyl constant. Variations at the **C aryl** included phenyl (ph), naphthyl (na), thiophenyl (th), and benzothiophenyl (bth), while the **peripheral N** group was thiazolyl (tz), benzothiazolyl (btz), or pyridyl (py). Similar [Pt(C^N^N)X] complexes had been previously reported, some of them showing high photoluminescence (PL) quantum yields at 289 K in solution, but no straightforward conclusion on structure–properties relations was drawn so far. We thus embarked to produce the above described series of [Pt(C^N^N)X] complexes and studied them in detail through an experimental and in-depth (TD)-DFT study.

Through variation of the donating character of the **C aryl** group and the π accepting abilities of the N^N moiety varied through the **peripheral N** group our complexes covered a broad range of electrochemical gaps from 1.7 to 2.6 eV between the first reductions and the first oxidations. At the same time similar gaps were found for pairs of complexes which contain structurally very different C^N^N ligands which is probably the result of electron-donating and -accepting effects compensating each other.

The experimental long-wavelength UV-vis absorption bands are markedly altered with the C^N^N variations with maxima ranging from 435 to 505 nm. The change in coligands generally leads to red-shifts in the maxima along the series Cl < C≡CC$_6$F$_5$ < C≡CPh. TD-DFT calculated spectra agree qualitatively well with the observed trends for the long-wavelength absorption bands, while the bands in the UV range were very well matched by the calculations.

Photoluminescence (PL) spectra at 298 K in CH$_2$Cl$_2$ show broad emissions peaking between 605 and 675 nm with quantum yields Φ_L ranging from <0.02 to 0.15. At 77 K, in frozen glassy matrices (CH$_2$Cl$_2$/MeOH 1:1), the PL spectra gain markedly in structure and show a general blue-shift of the maximum peak compared with the maximum of the broad bands at 298 K. The first maxima are found between 555 and 655 nm. As expected, the amplitude-weighted lifetimes τ_{av} increase from 0.39 to 2.18 μs at 298 K to 3.50 to 11.6 μs at 77 K.

The TD-DFT calculated emission spectra matched very well with the experimental spectra and the deconvolution showed excited states with pronounced LC (π–π*, centred in the individual parts of the C^N^N ligand) and LLCT (π–π*, between the individual parts of the C^N^N ligand) character, while MLCT (d$_{Pt}$-to-π*$_{C^N^N}$) (15%) and LMCT (p$_{Cl}$ or π$_{CCR}$-to-d$_{Pt}$) contributions are markedly lower.

In conclusion we can qualitatively confirm the often made quote that efficient triplet emitting Pt(ii) complexes show a high contribution (>50%) of ligand-centred states and a good contribution (>25%) of MLCT and LMCT states to the emitting triplet state. This combination makes the intersystem crossing fast and gives high quantum yields by boosting the phosphorescence rate from the lowest triplet state. At the same time, high ligand-centred contributions lead to high emission energies and can be easily traced by a high degree of vibronic progression of the emission bands. In turn, MLCT and LMCT contributions generally shorten the lifetimes. In our study we have deconvoluted the ligand-centred contributions to LC and

LLCT, which has allowed to trace the contributions to individual parts of the C^N^N ligand. Thus, we have identified several very interesting candidates for future applications. But more importantly, since the C^N^N ligands can be readily composed of different **C aryl**, **central N**, and **peripheral N** groups in a modular fashion, we can provide a rational to synthesise efficient triplet emitting Pt(ii) complexes. For the **central N** group, the (4-(3,5-di-*tert*-butyl)phenyl)-pyridyl was confirmed to be very useful. For the **C aryl** and **peripheral N** groups, the choice depends on the desired emission energy. The simple rule that the replacement of the Cl coligand by phenylacetylido (C≡CPh) or pentaflourophenylacetylido (C≡CC$_6$F$_5$) generally improves the emission efficiencies is not true in this case. The increased σ-donor character of the acetylido groups has to be well-matched with the σ-donor and π-acceptor properties of the C^N^N ligand to achieve efficient triplet emission. All in all, the approach of using these modular tridentate ligands + coligand, instead of sophisticated (laborous, low-yields) tetradentate ligands, has turned out to be very successful in providing efficiently phosphorescent Pt(ii) complexes. To evaluate their potential application, further PL measurements on the promising candidates (including those of previous studies) in solid matrices (*e.g.* PMMA) are necessary.

Experimental section

Materials

Reagents were purchased from Merck, Alfa Aesar, Acros Organics or abcr and used without further purification. Solvents (CH$_2$Cl$_2$, THF, toluene, diethyl ether and CH$_3$CN) were dried using an MBRAUN MB SPS-800 solvent purification system. Reactions which required the absence of air or moisture were performed under standard Schlenk technique. The protoligands and the Pt complexes are air-stable solids.

Syntheses

The synthesis and detailed characterisation of the ligand precursors, the HC^N^N protoligands and the Pt(ii) complexes is provided in the ESI† alongside with NMR spectra of ligands and Pt complexes (Fig. S001 to S074†).

Instrumentation

^{1}H, ^{13}C and ^{19}F NMR spectra were recorded on a Bruker Avance II 300 MHz ([1]H: 300.13 MHz, [13]C: 75.47 MHz) – double resonance (BBFO) 5 mm observe probehead with *z*-gradient coil, Bruker Avance 400 MHz ([1]H: 400.13 MHz, [13]C: 100.61 MHz, [19]F: 376.50 MHz) using a triple resonance ^{1}H, ^{19}F, BB inverse probe head or Bruker Avance II 600 MHz spectrometer ([1]H: 600.13 MHz, [13]C: 150.93 MHz) with a triple resonance (TBI) 5 mm inverse probehead with *z*-gradient coil using a triple resonance. The unambiguous assignment of the ^{1}H resonances was obtained from ^{1}H NOESY and ^{1}H COSY experiments. 2D NMR experiments were performed using standard pulse sequences from the Bruker pulse program library. Chemical shifts are relative to tetramethylsilane (TMS) respect-

ively. UV-vis absorption spectra were recorded with Varian Cary 05E or Cary 50 scan spectrophotometers. Photoluminescence spectra at room temperature were recorded with a Spex FluoroMax-3 spectrometer. A PicoQuant FluoTime 300 spectrometer was used for lifetime measurements. Lifetime analysis was performed using the commercial FluoFit software. The quality of the fit was assessed by minimising the reduced chi-squared function. Photoluminescence quantum yields (Φ_L) were determined with a Hamamatsu Photonics absolute PL quantum yield measurement system (C9920-02), equipped with a L9799-01 CW xenon light source, monochromator, photonic multichannel analyser and integrating sphere (an uncertainty of ±5% is estimated for Φ_L). All solvents were of spectroscopic grade. Both aerated samples and Ar-purged CH_2Cl_2 solutions were measured at 298 K in. Elemental analyses were obtained using a HEKAtech CHNS EuroEA 3000 analyzer. EI-MS spectra were measured with a Finnigan MAT 95, and HR-ESI-MS using a THERMO Scientific LTQ Orbitrap XL. Electrochemical measurements were carried out in 0.1 M $n\text{Bu}_4\text{NPF}_6$/THF solution using a three-electrode configuration (glassy carbon working electrode, Pt counter electrode, Ag/AgCl reference electrode) and a Metrohm Autolab PGSTAT30 or μStat 400 potentiostats. The ferrocene/ferrocenium couple served as internal reference. For electrochemical measurements extra dry solvents were used: extra dry DMF and CH_2Cl_2 was purchased from Acros Organics and stored over molecular sieve. THF was dried and destilled over Na/K (70/30) prior to use.

Single crystal X-ray diffractometric analysis

The data collection for $[Pd(th(ppy)py)Cl]\cdot CH_2Cl_2$ (**10·CH_2Cl_2**) was performed at $T = 170(2)$ K on a STOE IPDS II diffractometer (STOE and Cie., Darmstadt, Germany) with Mo-Kα radiation ($\lambda = 0.71073$ Å) employing ω–φ–2θ scan technique. The structures were solved by dual space methods (SHELXT-2015)[61] and refined by full-matrix least-squares techniques against F^2 (SHELXL-2017/1)[62,63] with $F_0{}^2 \geq 2\sigma(F_0{}^2)$. The numerical absorption correction (X-RED V1.31; STOE and Cie, 2005)[64] were performed after optimising the crystal shapes using X-SHAPE V1.06 (Stoe & Cie, 1999).[65] The structure of $[Pt(ph(tbppy)btz)(C\equiv CPh)]$ (**9**) was measured using synchrotron radiation ($\lambda = 0.56076$ Å) at 100(2) K, solved and refined without absorption correction as mentioned above. All non-hydrogen atoms were treated anisotropically; hydrogen atoms were included by using appropriate riding models. The dataset for **9** is generally poor and A alerts appeared in the checkcif. The problem is due to poor quality of the crystal. Nevertheless, we are convinced that the structure solution represents the geometric details of complex **9**. CCDC 2081667 $[Pd(th(ppy)py)Cl]\cdot CD_2Cl_2$ and 2084095 $[Pt(ph(tbppy)btz)(C\equiv CPh)]$† contains the full crystallographic data.

DFT calculations

The optimised geometries and the vibrational Franck–Condon spectra were determined with the quantum chemistry package Gaussian 09 Rev. D.01[66] using the CAM-B3LYP functional[67]

together with Grimme's D3 dispersion correction with Becke–Johnson damping.[68] The SDD basis set applies an effective core potential for the Pt atoms,[69] while the D95 basis set is used for H, C, N, and O atoms.[70]

To compute vibrational Franck–Condon spectra, the method of Barone et al.[71,72] with Kohn–Sham DFT-based geometry optimisations in the S_0 and T_1 states followed by frequency analysis calculations was used.

All energy corrections were done by adding zero-point vibrational energies and thermal free energy contributions. To calculate the overlap integrals for the vibronic spectra, the transitions are divided into classes Cn, where n is the number of the excited normal modes in the final electronic state. The number of quanta per mode was limited to 100 while the number of quanta for combinations of two modes was restricted to 65. The maximum number of computed integrals was set to 1.5×10^8. A maximum of 20 classes was calculated. The line spectrum was broadened with the aid of Gaussian functions with a half-width at half-maximum of 400 cm^{-1}.

The solvent CH_2Cl_2 was taken into account by the polarisable continuum model (PCM) in an integral equation formalism framework[73] with atomic radii from the universal force field model (UFF).[74] To characterise the emissive T_1 state, the T_1 geometry was first optimised with Kohn–Sham DFT with multiplicity 3 followed by TD-DFT calculations of the T_1 state. TD-DFT calculations of the 40 lowest excited singlet states were performed at the optimised S_0 geometry. Finally, a Lorentzian broadening with a half-width at half-maximum (HWHM) of 10 nm was used for each transition.

Conflicts of interest

There are no conflicts of interest to declare.

Acknowledgements

References

1 I. O. Koshevoy, M. Krause and A. Klein, Non-Covalent Intramolecular Interactions through Ligand-Design Promoting Efficient Luminescence from Transition Metal Complexes, *Coord. Chem. Rev.*, 2020, **405**, 213094.

2 G. Cheng, Y. Kwak, W.-P. To, T.-L. Lam, G. S. M. Tong, M.-K. Sit, S. Gong, B. Choi, W. Choi, C. Yang and C.-M. Che, High-Efficiency Solution-Processed Organic Light-Emitting Diodes with Tetradentate Platinum(II) Emitters, *ACS Appl. Mater. Interfaces*, 2019, **11**, 45161–45170.

3 G. Millán, N. Giménez, R. Lara, J. R. Berenguer, M. T. Moreno, E. Lalinde, E. Alfaro-Arnedo, I. P. López, S. Piñeiro-Hermida and J. G. Pichel, Luminescent Cycloplatinated Complexes with Biologically Relevant Phosphine Ligands: Optical and Cytotoxic Properties, *Inorg. Chem.*, 2019, **58**, 1657–1673.

4 A. I. Solomatina, P. S. Chelushkin, T. O. Abakumova, V. A. Zhemkov, M. Kim, I. Bezprozvanny, V. V. Gurzhiy, A. S. Melnikov, Y. A. Anufrikov, I. O. Koshevoy, S.-H. Su, P.-T. Chou and S. P. Tunik, Reactions of Cyclometalated Platinum(II) [Pt(N^C)(PR₃)Cl] Complexes with Imidazole and Imidazole-Containing Biomolecules: Fine-Tuning of Reactivity and Photophysical Properties via Ligand Design, *Inorg. Chem.*, 2019, **58**, 204–217.

5 L. Liu, X. Wang, F. Hussain, C. Zeng, B. Wang, Z. Li, I. Kozin and S. Wang, Multiresponsive Tetradentate Phosphorescent Metal Complexes as Highly Sensitive and Robust Luminescent Oxygen Sensors: Pd(II) Versus Pt(II) and 1,2,3-Triazolyl Versus 1,2,4-Triazolyl, *ACS Appl. Mater. Interfaces*, 2019, **11**, 12666–12674.

6 X. Wang and S. Wang, Phosphorescent Pt(II) Emitters for OLEDs: From Triarylboron-Functionalized Bidentate Complexes to Compounds with Macrocyclic Chelating Ligands, *Chem. Rec.*, 2019, **19**, 1–18.

7 Y. Zhang, Y. Wang, J. Song, J. Qu, B. Li, W. Zhu and W.-Y. Wong, Near-Infrared Emitting Materials via Harvesting Triplet Excitons: Molecular Design, Properties, and Application in Organic Light Emitting Diodes, *Adv. Opt. Mater.*, 2018, **6**, 1800466.

8 C. Cebrián and M. Mauro, Recent advances in phosphorescent platinum complexes for organic light-emitting diodes, *Beilstein J. Org. Chem.*, 2018, **14**, 1459–1481.

9 S. Wilde, D. Ma, T. Koch, A. Bakker, D. Gonzalez-Abradelo, L. Stegemann, C. D. Daniliuc, H. Fuchs, H. Gao, N. L. Doltsinis, L. Duan and C. A. Strassert, Toward Tunable Electroluminescent Devices by Correlating Function and Submolecular Structure in 3D Crystals, 2D-Confined Monolayers, and Dimers, *ACS Appl. Mater. Interfaces*, 2018, **10**, 22460–22473.

10 M. Krause, D. Kourkoulos, D. González-Abradelo, K. Meerholz, C. A. Strassert and A. Klein, Luminescent Pt^II Complexes of Tridentate Cyclometalating 2,5-Bis(aryl)-pyridine Ligands, *Eur. J. Inorg. Chem.*, 2017, **2017**, 5215–5223.

11 T. Fleetham, G. Li and J. Li, Phosphorescent Pt(II) and Pd(II) Complexes for Efficient, High-Color-Quality, and Stable OLEDs, *Adv. Mater.*, 2017, **29**, 1601861.

12 T.-T. Feng, F.-Q. Bai, L.-M. Xie, Y. Tang and H.-X. Zhang, Theoretical study and design of highly efficient platinum(II) complexes bearing tetradentate ligands for OLED, *RSC Adv.*, 2016, **6**, 11648–11656.

13 K. Li, G. S. M. Tong, Q. Wan, G. Cheng, W.-Y. Tong, W.-H. Ang, W.-L. Kwong and C.-M. Che, Highly phosphorescent platinum(II) emitters: photophysics, materials and biological application, *Chem. Sci.*, 2016, **7**, 1653–1673.

14 T. Strassner, Phosphorescent Platinum(II) Complexes with C^C* Cyclometalated NHC Ligands, *Acc. Chem. Res.*, 2016, **49**, 2680–2689.

15 J. Sanning, L. Stegemann, P. R. Ewen, C. Schwermann, C. G. Daniliuc, D. Zhang, N. Lin, L. Duan, D. Wegner, N. L. Doltsinis and C. A. Strassert, Colour-tunable asymmetric cyclometalated Pt(II) complexes and STM-assisted stability assessment of ancillary ligands for OLEDs, *J. Mater. Chem. C*, 2016, **4**, 2560–2565.

16 J. Zhao, W. Wu, J. Sun and S. Guo, Triplet photosensitizers: from molecular design to applications, *Chem. Soc. Rev.*, 2013, **42**, 5323–5351.

17 V. W.-W. Yam and K. M.-C. Wong, Luminescent metal complexes of d⁶, d⁸ and d¹⁰ transition metal centres, *Chem. Commun.*, 2011, **47**, 11579–11592.

18 H. Yersin, A. F. Rausch, R. Czerwieniec, T. Hofbeck and T. Fischer, The triplet state of organo-transition metal compounds. Triplet harvesting and singlet harvesting for efficient OLEDs, *Coord. Chem. Rev.*, 2011, **255**, 2622–2652.

19 J. A. G. Williams, The coordination chemistry of dipyridylbenzene: N-deficient terpyridine or panacea for brightly luminescent metal complexes?, *Chem. Soc. Rev.*, 2009, **38**, 1783–1801.

20 J. A. G. Williams, S. Develay, D. L. Rochester and L. Murphy, Optimising the luminescence of platinum(II) complexes and their application in organic light emitting devices (OLEDs), *Coord. Chem. Rev.*, 2008, **252**, 2596–2611.

21 J. Föller, D. H. Friese, S. Riese, J. M. Kaminski, S. Metz, D. Schmidt, F. Würthner, C. Lambert and C. M. Marian, On the photophysical properties of Ir^III, Pt^II, and Pd^II (phenylpyrazole) (phenyldipyrrin) complexes, *Phys. Chem. Chem. Phys.*, 2020, **22**, 3217–3233.

22 S. Poirier, H. Lynn, C. Reber, E. Tailleur, M. Marchivie, P. Guinneau and M. R. Probert, Variation of M···H−C Interactions in Square-Planar Complexes of Nickel(II), Palladium(II), and Platinum(II) Probed by Luminescence Spectroscopy and X-ray Diffraction at Variable Pressure, *Inorg. Chem.*, 2018, **57**, 7713–7723.

23 M. Krause, R. von der Stück, D. Brünink, S. Buss, N. L. Doltsinis, C. A. Strassert and A. Klein, Platinum and palladium complexes of tridentate ⁻C^N^N (phen-ide)-pyridine-thiazol ligands – A case study involving spectroelectrochemistry, photoluminescence spectroscopy and TD-DFT calculations, *Inorg. Chim. Acta*, 2021, **518**, 120093.

24 T. Eskelinen, S. Buss, S. K. Petrovskii, E. V. Grachova, M. Krause, L. Kletsch, A. Klein, C. A. Strassert, I. O. Koshevoy and P. Hirva, Photophysics and Excited State Dynamics of Cyclometalated $[M(C^\wedge N^\wedge N)(CN)]$ (M = Ni, Pd, Pt) Complexes: A Theoretical and Experimental Study, *Inorg. Chem.*, 2021, **60**, 8777–8789.

25 M. Hebenbrock, D. González-Abradelo, A. Hepp, J. Meadowcroft, N. Lefringhausen, C. A. Strassert and J. Müller, Influence of the ancillary ligands on the luminescence of platinum(II) complexes with a triazole-based tridentate $C^\wedge N^\wedge N$ luminophore, *Inorg. Chim. Acta*, 2021, **516**, 119988.

26 S. C. Gangadharappa, I. Maisuls, D. A. Schwab, J. Kösters, N. L. Doltsinis and C. A. Strassert, Compensation of Hybridization Defects in Phosphorescent Complexes with Pnictogen-Based Ligands-A Structural, Photophysical, and Theoretical Case-Study with Predictive Character, *J. Am. Chem. Soc.*, 2020, **142**, 21353–21367.

27 S. Garbe, M. Krause, A. Klimpel, I. Neundorf, P. Lippmann, I. Ott, D. Brünkink, C. A. Strassert, N. L. Doltsinis and A. Klein, Cyclometalated Pt Complexes of CNC Pincer Ligands: Luminescence and Cytotoxic Evaluation, *Organometallics*, 2020, **39**, 746–756.

28 Y. Luo, Z. Chen, J. Hu, Z. Xu, Q. Meng and D. Tang, Small substituent groups as geometric controllers for tridentate platinum(II) complexes to effectively suppress non-radiative decay processes, *Phys. Chem. Chem. Phys.*, 2019, **21**, 2764–2770.

29 Y.-T. Liu, Y.-R. Li, X. Wang and F.-Q. Bai, Theoretical investigation of $N^\wedge C^\wedge N$-coordinated Pt(II) and Pd(II) complexes for long-lived two-photon photodynamic therapy, *Dyes Pigm.*, 2017, **142**, 55–61.

30 R. Mroz, D. A. K. Vezzu, B. Wallace, D. Ravindranathan, J. Carroll, R. D. Pike and S. Huo, A Comparative Study on Phosphorescent Cycloplatinated Complexes Based on Tridentate $C^\wedge N^\wedge N$-Coordinating Ligands and Phenylethynyl or Phenyl Ligand, *Chin. J. Org. Chem.*, 2018, **38**, 171–182.

31 P.-K. Chow, G. Cheng, G. S. M. Tong, W.-P. To, W.-L. Kwong, K.-H. Low, C.-C. Kwok, C. Ma and C.-M. Che, Luminescent Pincer Platinum(II) Complexes with Emission Quantum Yields up to Almost Unity: Photophysics, Photoreductive C-C Bond Formation, and Materials Applications, *Angew. Chem., Int. Ed.*, 2015, **54**, 2084–2089.

32 P. Wu, E. L.-M. Wong, D.-L. Ma, G. S.-M. Tong, K.-M. Ng and C.-M. Che, Cyclometalated Platinum(II) Complexes as Highly Sensitive Luminescent Switch-On Probes for Practical Application in Protein Staining and Cell Imaging, *Chem. – Eur. J.*, 2009, **15**, 3652–3656.

33 S. C. F. Kui, F.-F. Hung, S.-L. Lai, M.-Y. Yuen, C.-C. Kwok, K.-H. Low, S. S.-Y. Chui and C.-M. Che, Luminescent Organoplatinum(II) Complexes with Functionalized Cyclometalated $C^\wedge N^\wedge C$ Ligands: Structures, Photophysical Properties, and Material Applications, *Chem. – Eur. J.*, 2012, **18**, 96–109.

34 L. Wang, Y. Zhang, J. Li, H. He and J. Zhang, Influence of primary and auxiliary ligand on spectroscopic properties and luminescent efficiency of organoplatinum(II) complexes bearing functionalized cyclometalated $C^\wedge N^\wedge C$ ligands, *Dalton Trans.*, 2014, **43**, 14029–14038.

35 I. Maisuls, C. Wang, M. E. Gutierrez Suburu, S. Wilde, C.-G. Daniliuc, D. Brünink, N. L. Doltsinis, S. Ostendorp, G. Wilde, J. Kösters, U. Resch-Genger and C. A. Strassert, Ligand-controlled and nanoconfinement-boosted luminescence employing Pt(II) and Pd(II) complexes: from color-tunable aggregation-enhanced dual emitters towards self-referenced oxygen reporters, *Chem. Sci.*, 2021, **12**, 3270–3281.

36 D. Qiu, J. Wu, Z. Xie, Y. Cheng and L. Wang, Synthesis, photophysical and electrophosphorescent properties of mononuclearPt(II) complexes with arylamine functionalized cyclometalating ligands, *J. Organomet. Chem.*, 2009, **694**, 737–746.

37 M. Hruzd, N. le Poul, M. Cordier, S. Kahlal, J.-Y. Saillard, S. Achelle, S. Gauthier and F. Robin-le Guen, Luminescent cyclometalated alkynylplatinum(II) complexes with 1,3-di(pyrimidin-2-yl)benzene ligands: synthesis, electrochemistry, photophysics and computational studies, *Dalton Trans.*, 2022, **51**, 5546–5560.

38 G. De Soricellis, F. Fagnani, A. Colombo, C. Dragonetti and D. Roberto, Exploring the potential of $N^\wedge C^\wedge N$ cyclometalated Pt(II) complexes bearing 1,3-di(2-pyridyl)benzene derivatives for imaging and photodynamic therapy, *Inorg. Chim. Acta*, 2022, **541**, 121082.

39 W. Cai, H. Zhang, X. Yan, A. Zhao, R. He, M. Li, Q. Meng and W. Shen, What accounts for the color purity of tetradentate Pt complexes? A computational analysis, *Phys. Chem. Chem. Phys.*, 2019, **21**, 8073–8080.

40 M. Cnudde, D. Brünink, N. L. Doltsinis and C. A. Strassert, Tetradentate $N^\wedge N^\circ N^\wedge N$-type luminophores for Pt(II) complexes: Synthesis, photophysical and quantum-chemical investigation, *Inorg. Chim. Acta*, 2021, **518**, 120090.

41 L. Wang, J. Wen, H. He and J. Zhang, The reasons for ligand-dependent quantum yields and spectroscopic properties of platinum(II) complexes based on tetradentate $O^\wedge N^\wedge C^\wedge N$ ligands: a DFT and TD-DFT study, *Dalton Trans.*, 2014, **43**, 2849–2858.

42 G. S.-M. Tong and C.-M. Che, Emissive or Nonemissive? A Theoretical Analysis of the Phosphorescence Efficiencies of Cyclometalated Platinum(II) Complexes, *Chem. – Eur. J.*, 2009, **15**, 7225–7237.

43 B. Yang, S. Huang and J. Wang, How do ligands influence the quantum yields of cyclometalated platinum(II) complexes, theoretical research study, *Phys. Chem. Chem. Phys.*, 2017, **19**, 23454–23460.

44 W. Li, J. Wang, X. Yan, H. Zhang and W. Shen, Electronic structures and photophysical properties of phosphorescent platinum(II) complexes with tridentate $C^\wedge N*N$ cyclometalated ligands, *Appl. Organomet. Chem.*, 2018, **32**, e3929.

45 A. Heil and C. M. Marian, Structure−Emission Property Relationships in Cyclometalated Pt(II) β-Diketonate Complexes, *Inorg. Chem.*, 2019, **58**, 6123–6136.

46 H. Kurz, K. Schötz, I. Papadopoulos, F. W. Heinemann, H. Maid, D. M. Guldi, G. Hörner and B. Weber, A

Fluorescence-Detected Coordination-Induced Spin State Switch, *J. Am. Chem. Soc.*, 2021, **143**, 3466–3480.

47 M. L. Clark, S. Diring, P. Retailleau, D. R. McMillin and R. Ziessel, Spectroscopic Properties of Orthometalated Platinum(II) Bipyridine Complexes Containing Various Ethynylaryl Groups, *Chem. – Eur. J.*, 2008, **14**, 7168–7179.

48 V. Lingen, A. Lüning, C. Strauss, I. Pantenburg, G. B. Deacon, G. Meyer and A. Klein, Platinum Complexes with the SC_6F_4H-4 Ligand – Synthesis, Spectroscopy and Structures, *Inorg. Chim. Acta*, 2014, **423**, 152–162.

49 G.-J. Zhang, X. Gan, Q.-Q. Xu, Y. Chen, X.-J. Zhao, B. Qin, X.-J. Lv, S.-W. Lai, W.-F. Fu and C.-M. Che, Photophysical and electrochemical properties of platinum(II) complexes bearing a chromophore–acceptor dyad and their photocatalytic hydrogen evolution, *Dalton Trans.*, 2012, **41**, 8421–8429.

50 M.-Y. Yuen, S. C. F. Kui, K.-H. Low, C.-C. Kwok, S. S.-Y. Chui, C.-W. Ma, N. Zhu and C.-M. Che, Synthesis, Photophysical and Electrophosphorescent Properties of Fluorene-Based Platinum(II) Complexes, *Chem. – Eur. J.*, 2010, **16**, 14131–14141.

51 K. Li, T. Zou, Y. Chen, X. Guan and C.-M. Che, Pincer-Type Platinum(II) Complexes Containing N-Heterocyclic Carbene (NHC) Ligand: Structures, Photophysical and Anion-Binding Properties, and Anticancer Activities, *Chem. – Eur. J.*, 2015, **21**, 7441–7453.

52 R. P.-L. Tang, K. M.-C. Wong, N. Zhu and V. W.-W. Yam, Luminescence, electrochemistry and host–guest properties of dinuclear platinum(II) terpyridyl complexes of sulfur-containing bridging ligands, *Dalton Trans.*, 2009, **2009**, 3911–3922.

53 A. Klein, J. van Slageren and S. Záliš, Co-ligand involvement in ground and excited states of electron rich polypyridyl platinum(II) complexes, *Eur. J. Inorg. Chem.*, 2003, **2003**, 1917–1938.

54 S.-C. Chan, M. C. W. Chan, Y. Wang, C.-M. Che, K.-K. Cheung and N. Zhu, Organic Light-Emitting Materials Based on Bis(arylacetylide)platinum(II) Complexes Bearing Substituted Bipyridine and Phenanthroline Ligands: Photo- and Electroluminescence from [3]MLCT Excited States, *Chem. – Eur. J.*, 2001, **7**, 4180–4190.

55 J. van Slageren, A. Klein, S. Záliš and D. J. Stufkens, Resonance Raman spectra of d^6 metal-diimine complexes reflect changes in metal-ligand interaction and character of electronic transitions, *Coord. Chem. Rev.*, 2001, **219–221**, 937–955.

56 T.-C. Cheung, K.-K. Cheung, S.-M. Peng and C.-M. Che, Photoluminescent cyclometallated diplatinum(II,II) complexes: photophysical properties and crystal structures of [PtL(PPh₃)]ClO₄ and [Pt₂L₂(μ-dppm)][ClO₄] (HL = 6-phenyl-2,2′-bipyridine, dppm = Ph₂PCH₂PPh₂), *J. Chem. Soc., Dalton Trans.*, 1996, **1996**, 1645–1651.

57 W. Lu, B.-X. Mi, M. C. W. Chan, Z. Hui, C.-M. Che, N. Zhu and S.-T. Lee, Light-Emitting Tridentate Cyclometalated Platinum(II) Complexes Containing σ-Alkynyl Auxiliaries: Tuning of Photo- and Electrophosphorescence, *J. Am. Chem. Soc.*, 2004, **126**, 4958–4971.

58 W. Lu, M. C. W. Chan, N. Zhu, C.-M. Che, Z. He and K.-Y. Wong, Structural Basis for Vapoluminescent Organoplatinum Materials Derived from Noncovalent Interactions as Recognition Components, *Chem. – Eur. J.*, 2003, **9**, 6155–6166.

59 A. Sillen and Y. Engelborghs, The Correct Use of "Average" Fluorescence Parameters, *Photochem. Photobiol.*, 1998, **67**, 475–486.

60 F. Plasser, TheoDORE: A toolbox for a detailed and automated analysis of electronic excited state computations, *J. Chem. Phys.*, 2020, **152**(8), 84108.

61 G. M. Sheldrick, ShelXT – Integrated space-group and crystal-structure determination, *Acta Crystallogr., Sect. A: Found. Crystallogr.*, 2015, **71**, 3–8.

62 G. M. Sheldrick, *SHELXL-2017/1, Program for the Solution of Crystal Structures*, University of Göttingen, Göttingen, Germany, 2017.

63 G. M. Sheldrick, Crystal structure refinement with SHELXL, *Acta Crystallogr., Sect. C: Struct. Chem.*, 2015, **71**, 3–8.

64 *STOE X-RED, Data Reduction Program, Version 1.31/Windows*, STOE & Cie, Darmstadt, Germany, 2005.

65 *STOE X-SHAPE, Crystal Optimisation for Numerical Absorption Correction, Version 1.06/Windows*, STOE & Cie, Darmstadt, Germany, 1999.

66 M. J. Frisch, G. W. Trucks, H. B. Schlegel, G. E. Scuseria, M. A. Robb, J. R. Cheeseman, G. Scalmani, V. Barone, B. Mennucci, G. A. Petersson, *et al.*, *Gaussian 09, Revision D.01. 2009*, Gaussian Inc., Wallingford CT, 2009.

67 T. Yanai, D. P. Tew and N. C. Handy, A new hybrid exchange–correlation functional using the Coulomb-attenuating method (CAM-B3LYP), *Chem. Phys. Lett.*, 2004, **293**, 51–57.

68 S. Grimme, S. Ehrlich and L. Goerigk, Effect of the damping function in dispersion corrected density functional theory, *J. Comput. Chem.*, 2011, **32**, 1456–1465.

69 D. Andrae, U. Häußermann, M. Dolg, H. Stoll and H. Preuß, Energy-adjusted ab initio pseudopotentials for the second and third row transition elements, *Theor. Chim. Acta*, 1990, **77**, 123–141.

70 T. H. Dunning and P. J. Hay, in *Modern Theoretical Chemistry*, ed. H. F. Schaefer III, Plenum, New York, 1976, Vol. 3, pp. 1–28.

71 V. Barone, J. Bloino and M. Biczysko, *Vibrationally-resolved electronic spectra in GAUSSIAN 09, GAUSSIAN 09 Revision A.02*, 2009, 1–20.

72 V. Barone, J. Bloino, M. Biczysko and F. Santoro, Fully Integrated Approach to Compute Vibrationally Resolved Optical Spectra: From Small Molecules to Macrosystems, *J. Chem. Theory Comput.*, 2009, **5**, 540–554.

73 J. Tomasi, B. Mennucci and R. Cammi, Quantum Mechanical Continuum Solvation Models, *Chem. Rev.*, 2005, **105**, 2999–3094.

74 W. M. Skid, UFF, a Full Periodic Table Force Field for Molecular Mechanics and Molecular Dynamics Simulations, *J. Am. Chem. Soc.*, 1992, **114**, 10024–10035.